LAWRENCE
LIVERMORE
NATIONAL
LABORATORY

LLNL-TR-666244

Nudged Elastic Band Simulations of Kink Pairs in Tungsten

D. Cereceda, J. Marian

January 16, 2015

Disclaimer

This work performed under the auspices of the U.S. Department of Energy by Lawrence Livermore National Laboratory under Contract DE-AC52-07NA27344.

NUDGED ELASTIC BAND SIMULATIONS OF KINK PAIRS IN TUNGSTEN -- David Cereceda and Jaime Marian (Lawrence Livermore National Laboratory and University of California at Los Angeles)

OBJECTIVE

The objective of this work is to calculate properties of tungsten at the atomistic level that are key to predicting the yield stress and flow stress of the material.

SUMMARY

Atomistic techniques have been used to calculate energy barriers for dislocation motion that control the strength (yield stress and flow stress) of the material. In particular, the calculations focus on the change in enthalpy as a straight dislocation moves through the crystal lattice (the Peierls barrier) and kink pair formation enthalpy that controls the thermally activated double-kink mechanism important at low to moderate stresses. A novel means of assessing kink widths within atomistic simulations is introduced.

PROGRESS AND STATUS

1 Introduction

The movement of dislocations can be considered as a set of successive processes that define a pathway through the potential energy landscape. Each of these processes happens between two configurations of atoms that are local minima corresponding to straight dislocations in equilibrium, providing information about the activation energy of the process and what intermediate equilibrium configurations may exist along the transition.

The nucleation and propagation of kink pairs between these local minima appears to be one of the underlying mechanisms that explain some of the characteristics of the motion of dislocations.

Below, we describe the general ideas on how these processes are studied by the 'nudged elastic band' (NEB) method discussed in more detail by Henkelman et al. [1] and by Tadmor and Miller in section 6.3.1 of the book *Modeling Materials* [2].

In the NEB method, a replica of a system with N atoms is defined by a N × 3 matrix that contains the positions of all the atoms in the system, $\mathbf{P} = (\mathbf{r}^1, \mathbf{r}^2, ..., \mathbf{r}^N)$. Given a total number of *R* replicas to study the movement of a dislocation between two consecutive Peierls valleys, the first and last replicas, P^1 and P^R, are at local energy minima in the energy landscape. All the other intermediate replicas can be characterized in different ways, but they are not in equilibrium, exhibiting a force on the atoms of each replica *i* that comes from the non-zero gradient of the potential energy

$$\mathbf{F}^i_{pot} = -\nabla_P V(\mathbf{P}^i) = \{-\nabla_{r^1} V|_{P^i}, ..., -\nabla_{r^N} V|_{P^i}\} \qquad (1)$$

The minimization of these forces would displace each intermediate replica to one of the local minima. In the NEB method, replicas 1 and R are fixed, and each intermediate replica is connected to the previous and next replica by a spring of constant k. These springs introduce a new force F^i_{spring} that depends on the value of the spring constant. If k is small, the spring forces will not affect the minimization and the replicas will fall to one of the local minima. If k is big, the replicas are more rigid, and the spring forces will define a higher-energy path.

Considering the combined action of these two types of forces, the 3N-dimensional force on replica *i*, F^i, is defined as

$$\mathbf{F}^i = \mathbf{F}^i_{pot}|_\perp + \mathbf{F}^i_{spring}|_\parallel, \qquad (2)$$

where

$$\mathbf{F}^i_{pot}|_\perp = \mathbf{F}^i_{pot} - (\mathbf{F}^i_{pot} \cdot \mathbf{t}^i)\mathbf{t}^i, \qquad \mathbf{F}^i_{spring}|_\parallel = k(\|\mathbf{P}^{i+1} - \mathbf{P}^i\| - \|\mathbf{P}^i - \mathbf{P}^{i-1}\|)\mathbf{t}^i,$$

t^i is the 3N-dimensional tangent to the path at replica *i*, $\mathbf{F}^i_{pot}|_\perp$ is the component of the forces derived from the potential energy that is perpendicular to the path and $\mathbf{F}^i_{spring}|_\parallel$ is the component of the spring forces acting parallel to the path. In this distribution of forces, $\mathbf{F}^i_{pot}|_\perp$ will attempt to move each replica vertically to the minima and $\mathbf{F}^i_{spring}|_\parallel$ will attempt to move it along the reaction coordinate. The minimum energy path (MEP) between Peierls valleys can now be obtained by running an algorithm that moves the atomistic configurations of all the replicas until the global force defined in Eq.2 is reduced to zero.

2 Computational details

The principal axes x, y, and z, of the simulation box were oriented along the $\frac{1}{2}[111]$, $[\bar{1}2\bar{1}]$, and $[\bar{1}01]$ directions, corresponding to the line, glide and normal directions, respectively, of the screw dislocation. The dimensions of the simulation box were chosen to maximize the physical fidelity of the results while keeping the computational cost manageable. According to these criteria the dimensions are: L_x = 27.2 nm (100 b), L_y =10.8 nm, and L_z = 10.7 nm, with a total number of 208300 atoms.

Two screw dislocations with Burgers vector **b** = $\frac{1}{2}[111]$ are generated by using the isotropic elastic displacement solution [3] in two independent simulation boxes (one dislocation per box) with the orientation and dimensions described before. The first dislocation d_1 is generated at the center of the box. The second dislocation d_2 is generated at a distance[1] of $\frac{\sqrt{6}}{3}a_0$ from the center of the simulation box along the glide direction $[\bar{1}2\bar{1}]$, which corresponds to the distance between two consecutive Peierls valleys in that direction.

Prior to the NEB simulations, dislocations d_1 and d_2 are relaxed using the conjugate gradient algorithm implemented in LAMMPS [4]. Periodic boundary conditions are applied in the x direction while non-periodic and shrink-wrapped boundary conditions are applied in the y and z directions.

A stress range from zero to the Peierls stress of the potential is studied by applying shear stress σ_{xz}. To reproduce the effect of this applied stress, a external force f_x is added to the atoms in the top and bottom surfaces along the normal direction $[\bar{1}01]$.

[1] a_0 is the lattice parameter of the interatomic potential used in the simulations.

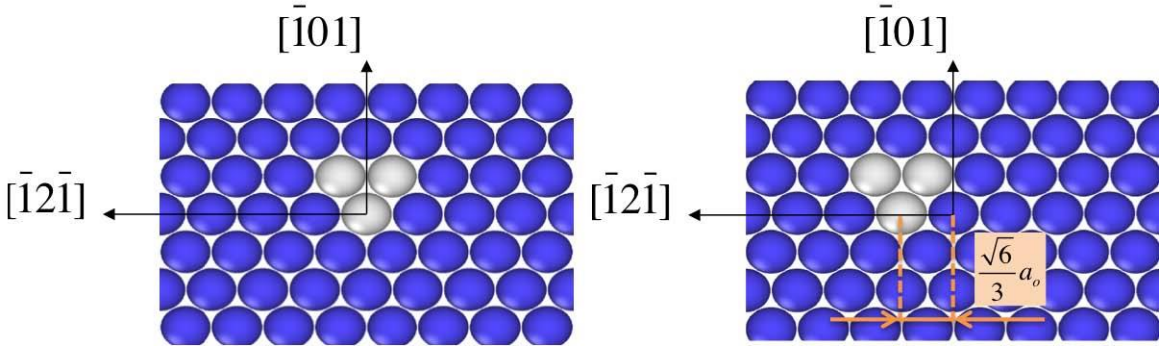

(a) dislocation d_1 (b) dislocation d_2

Figure 1: Position of the first d1 and second d2 dislocation with (1 0 1) plane.

The external force per atom satisfies $f_x = \frac{\sigma L_x L_y}{N_s}$, where σ is the desired stress and N_s is the number of atoms in each surface.

The MEP is obtained using the NEB method described before [1, 4, 5, 6, 7]. In this work we present two different types of NEB simulations depending on the intermediate configurations: straight dislocations or kink-pairs. Both of them use a total of 31 replicas, a spring constant of 1 eV $Å^{-1}$ and set relaxed dislocations d_1 and d_2 as the initial (1) and final (R) configurations respectively.

In this work we have used two different interatomic potential parameterized for tungsten: an embedded-atom method (EAM) potential [8] and a modified embedded-atom method (MEAM) potential [9]. Both of them predict the correct symmetric core structure at 0 K. They predict a Peierls stress of 2.03 and 3.2 GPa, respectively.

3 Results

3.1 Enthalpy and Energy Barriers

Straight dislocations

For the study of a straight dislocation moving between two consecutive Peierls valleys along the glide direction, the initial coordinates of all the atoms in the intermediate replica i, P^i_0, are set to values linearly interpolated between the corresponding atoms in replicas 1 and R.

$$\mathbf{P}_0^i = \mathbf{P}^1 + \frac{i-1}{R-1}\left(\mathbf{P}^R - \mathbf{P}^1\right), \tag{3}$$

where i=2 . . . R-1.Therefore, the initial path of the NEB simulation contains a single dislocation for every replica.

The dimension along the dislocation line is reduced to L_x = 1.36 nm (5 b). In contrast with the study of kink-pairs where a value of L_x = 27.2 nm (100 b) is required for the nucleation of the kinks, this reduced size of the box is big enough for the straight dislocation to reproduce the physical fidelity of the results while decreasing the computational cost of the simulations.

For a given replica *i*, its enthalpy, H_i, includes the contribution of the internal energy and the mechanical work generated by the applied stress

$$H_i = U_i - \sigma \cdot b \cdot L_x \cdot \theta_r, \tag{4}$$

where U_i is the internal energy of the replica, σ is the applied stress and θ_r is the reaction coordinate along the MEP. The enthalpy barrier per unit length is represented in Fig.2 as the difference between the enthalpy of each replica and the enthalpy of the initial configuration of the NEB simulation. One can notice that the increase in the applied stress increases the negative slope of the enthalpy barrier and decreases the maximum value achieved.

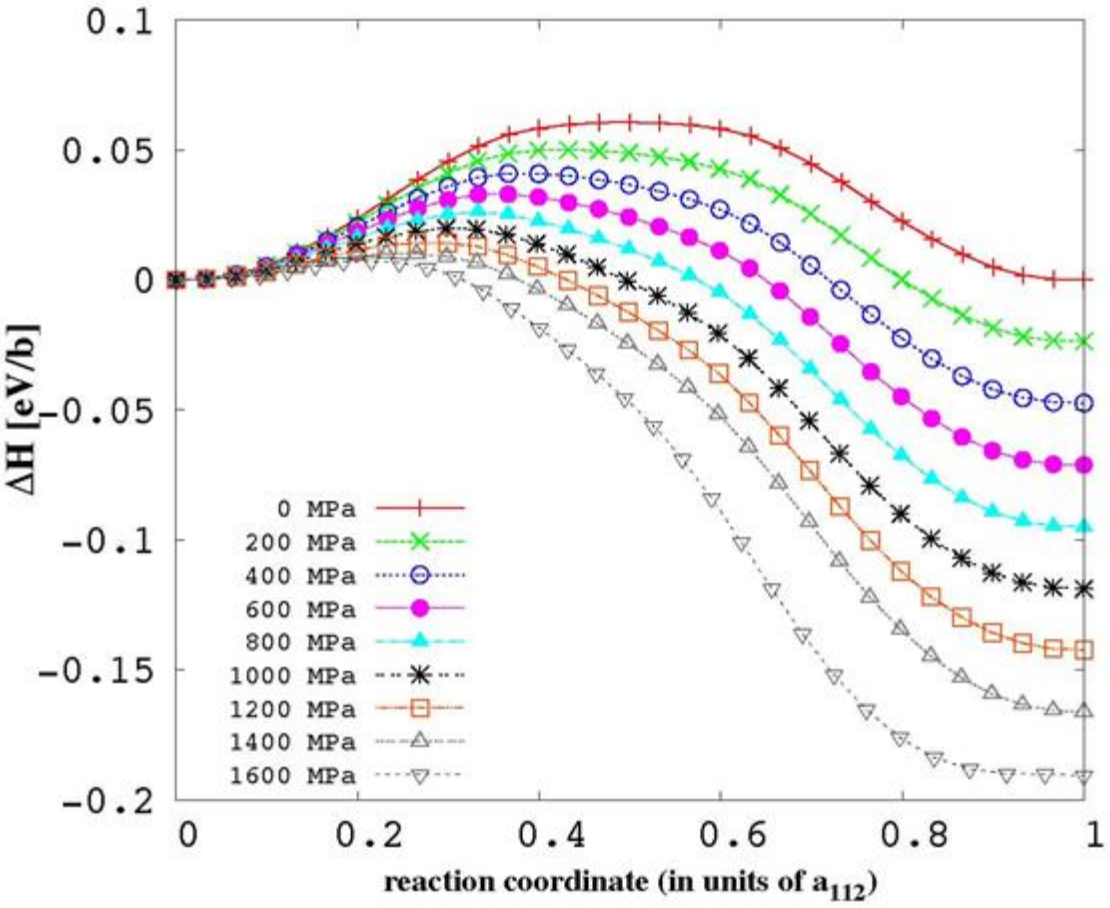

Figure 2: Enthalpy barrier per Burgers vector for a straight screw dislocation with normal plane $[\bar{1}01]$, computed with the NEB method using the EAM potential under the full range of applied stress.

According to Eq.4, the energy barrier is obtained by adding the mechanical work to the enthalpy. Similar to the enthalpy barrier, the energy barrier per unit length is represented in Fig.3.a as the difference between the energy of each replica and the energy of the initial configuration of the NEB simulation. In Fig.3.b, energies and reaction coordinates were shifted to overlap the potential minima for the different applied stresses [10].

In addition to the study of the $\frac{1}{2}<111>\{110\}$ screw dislocation, the Peierls potential for the $\frac{1}{2}<111>\{112\}$ screw dislocation was also studied. In this case the directions $\frac{1}{2}[111]$, $[\bar{1}01]$, and $[\bar{1}2\bar{1}]$ correspond to the line, glide and normal directions of the simulation box, respectively. The second dislocation d_2 is generated at a distance of $\sqrt{2}a_0$ from the center of the simulation box along the new glide direction $[\bar{1}01]$. For this orientation of the system Fig4.b shows a MEP with two barriers to move the straight dislocation between two consecutive Peierls valleys along the (1 2 1) plane. These results, in addition to the results of Fig.5.a, where the energy barriers along the $(10\bar{1})$ and $(\bar{1}2\bar{1})$ planes are plotted together at 0 MPa, suggest that the MEP along the $(\bar{1}2\bar{1})$ plane can be explained as two partial MEP along the x plane. Therefore the study of the kink-pair enthalpy has been completed only for the $\frac{1}{2}<111>\{110\}$ system.

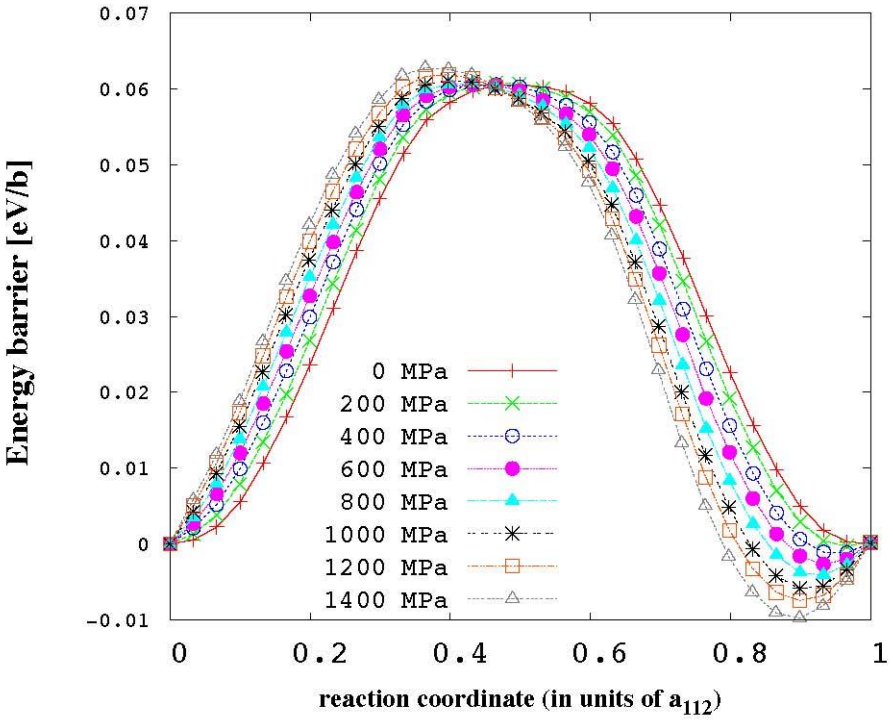

(a)

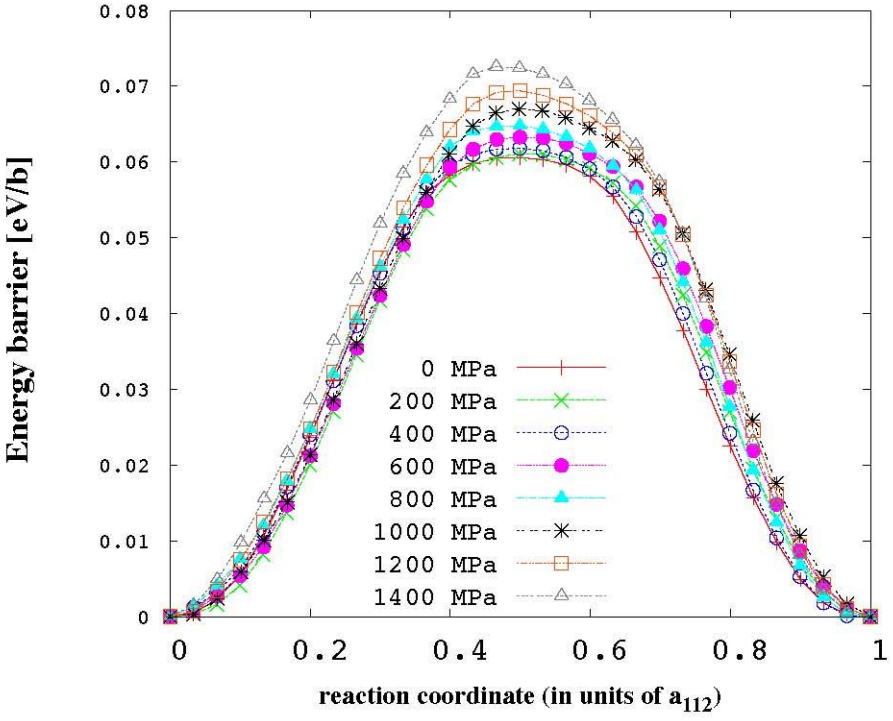

(b)

Figure 3: Energy barrier per Burgers vector for a straight screw dislocation with normal plane $(10\bar{1})$ and EAM potential.

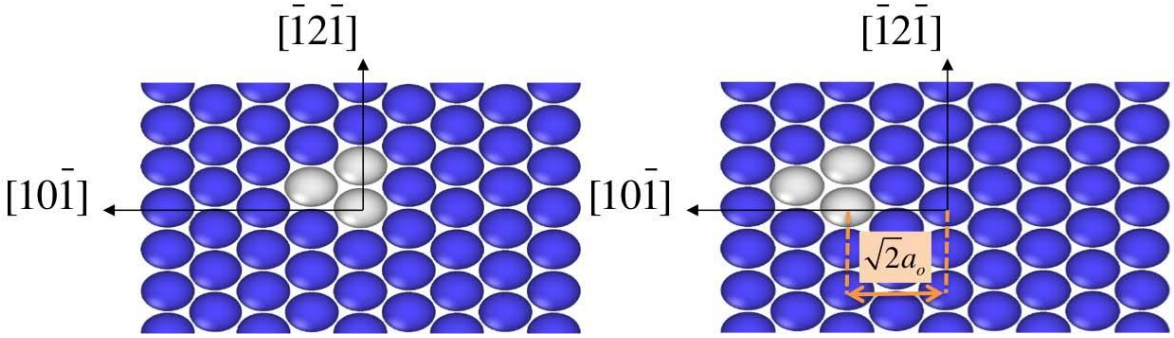

(a)

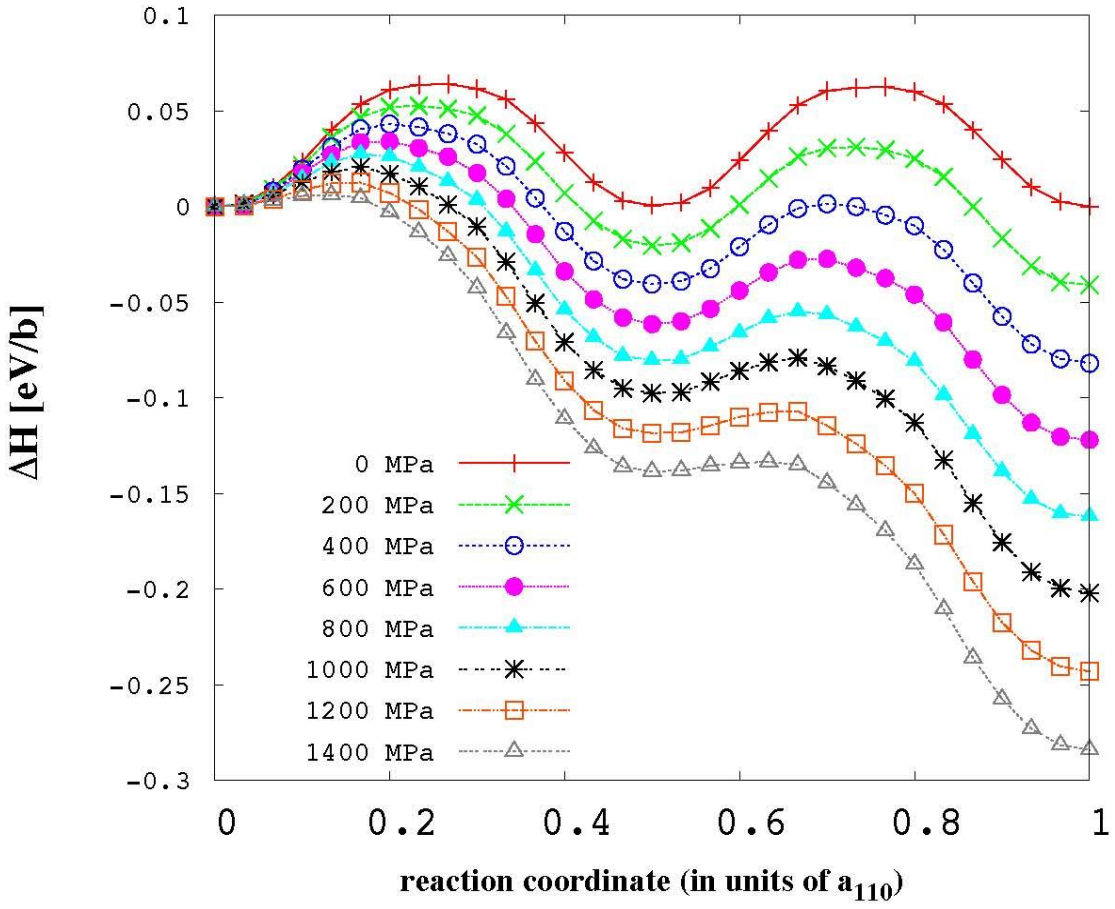

(b)

Figure 4: (a) Position of dislocations d_1 and d_2 when the screw is oriented with $(\bar{1}2\bar{1})$ as the normal plane. (b) Enthalpy barrier per Burgers vector for a straight screw dislocation with normal plane $(\bar{1}2\bar{1})$, computed with the NEB method using the EAM potential.

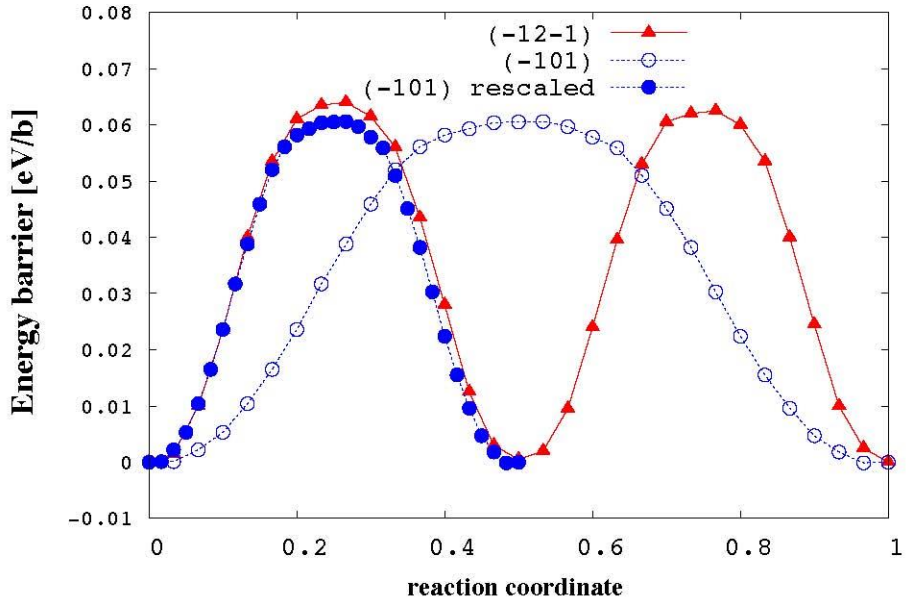

(a) EAM potential

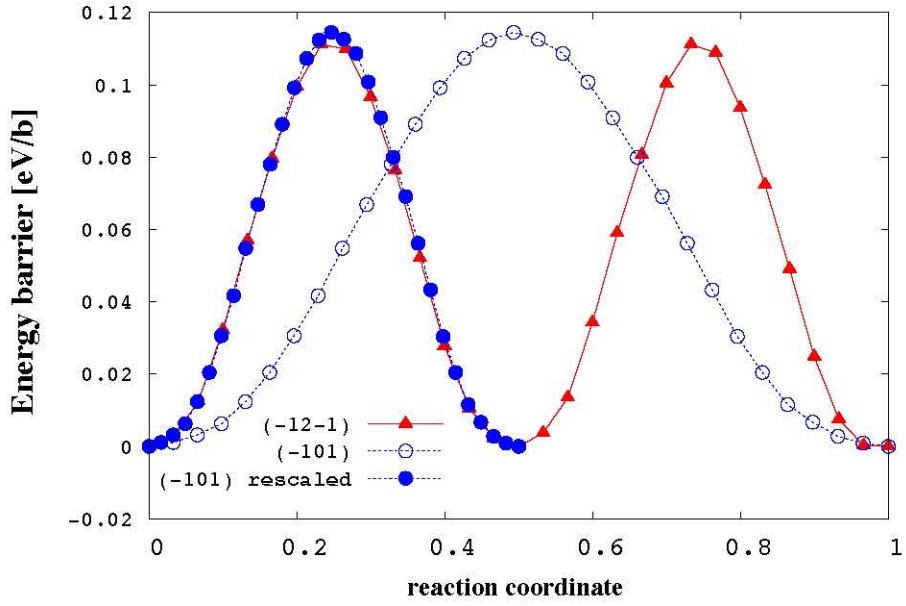

(b) MEAM potential

Figure 5: Energy barrier at 0 MPa for the $(10\bar{1})$ and $(\bar{1}2\bar{1})$ planes versus the reaction coordinate in units of the glide direction, $[\bar{1}2\bar{1}]$and $[10\bar{1}]$ respectively.

The enthalpy and energy barriers have also been computed for more accurate and more expensive [11] MEAM potential. The results of Fig.6.b and the comparison between Fig.5.a and Fig.5.b reflect a more sinusoidal behavior of the MEAM potential, in agreement with the results of all the bcc transition metals [12].

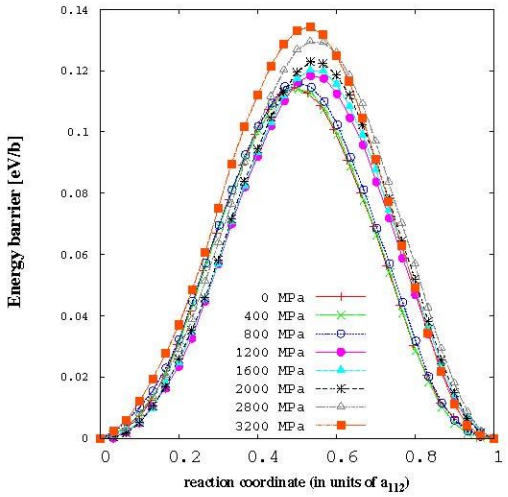

(c) Energy barrier (shifted)

Figure 6: Enthalpy and energy barriers versus the reaction coordinate in units of the glide direction, $[\bar{1}2\bar{1}]$, for the MEAM potential.

Kink-pairs

For the study of the enthalpy and energy barriers in kink-pairs, the initial configurations of the intermediate replicas 2, 3, …, R-1 contain a kink pair in the simulation box. The width of the kink pair *w* depends on the number of the replica *i* as follows

$$w_i = 0.5\left(1 + \frac{i-2}{R-2}\right) L_x, \tag{5}$$

where *i*=2 . . . R-1. The initial coordinates of the atoms in the intermediate replicas correspond to the initial configuration except for a region of width w_i around the YZ central plane where atomic positions are taken from the final configuration [13].

In this case, the initial path of the NEB simulation contains a single dislocation for the initial and final replica, and a kink pair for the intermediate replicas 2 . . . R-1.

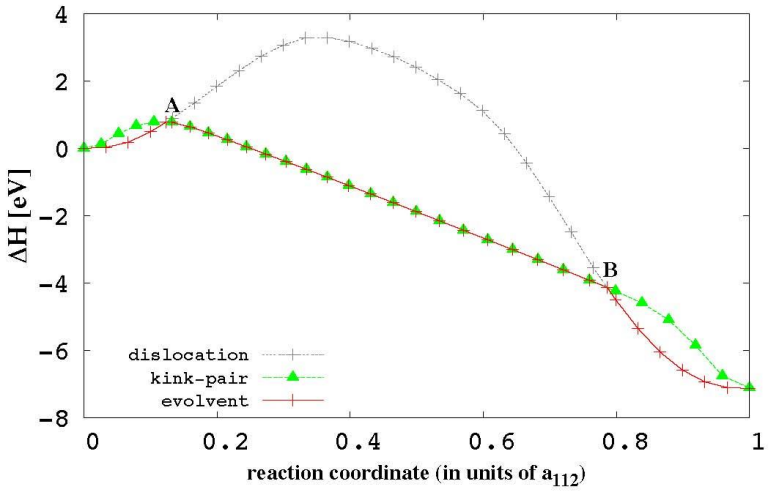

Figure 7: Enthalpy barrier when the initial configurations of the intermediate replicas are straight dislocations, kink-pairs, and the resultant envelope of minimum enthalpy of this two cases for the EAM potential at 600 MPa.

For each value of applied stress, the real pathway between two consecutive Peierls valleys is defined by the envelope of minimum enthalpy when overlapping the enthalpy barriers of the straight dislocation and the kink-pair.

$$H_{MEP}(i) = \begin{cases} H_{disloc}(i) & \text{if } H_{disloc}(i) \leq H_{kp}(i) \\ H_{kp}(i) & \text{if } H_{disloc}(i) < H_{kp}(i) \end{cases}, \tag{6}$$

where $H_{MEP}(i)$ is the enthalpy of the replica *i* defined by the MEP, $H_{disloc}(i)$ is the enthalpy of the replica *i* at the end of the NEB simulation when the initial configurations of the intermediate replicas are straight dislocations and $H_{kp}(i)$ is the enthalpy of the replica *i* at the end of the NEB simulation when the initial configurations of the intermediate replicas are kink-pairs.

The point *A* in Fig.7 where the enthalpy barriers of the straight dislocation and the kink-pair intersect represents the state where the kink-pair is nucleated, and it defines, for a specific applied stress, the enthalpy and width of the kink-pair. The point *B* where the enthalpy barriers of the straight dislocation and the kink-pair also intersect, but in this case with a negative slope, represents the state where the kink-pair is totally expanded and becomes a straight dislocation situated in the next Peierls valley. All the replicas in the segment *AB* contain a kink-pair with an increased width.

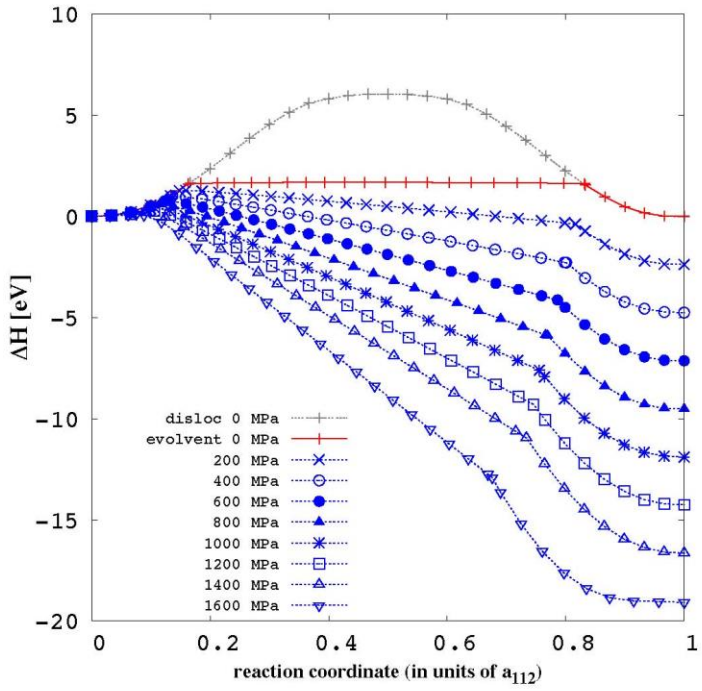

Figure 8: Enthalpy barrier of the straight dislocation at 0 MPa and the envelope of minimum enthalpy for the full range of applied stress 0 -1600 MPa and EAM potential.

3.2 Kink-Pair Enthalpy

The interest of obtaining the kink-pair enthalpy as a function of the stress comes from the important role that this variable plays when defining the nucleation rate of a kink-pair, j_{kp}. This nucleation rate can be defined as:

$$j_{kp} = \nu_0 exp\left\{-\frac{\Delta F_{kp}}{2kT}\right\} \tag{7}$$

where ν_0 is an attempt frequency, k is Boltzmann's constant, T is the temperature and ΔF_{kp} is the (Gibbs) free energy difference resulting from the nucleation of an embryonic kink pair, i.e. one with the minimum lattice separation. The 1/2 factor arises from the fact that it is only necessary to take the dislocation to the activated state (saddle point) to achieve a transition. This is only appropriate for cases where the free energy landscape is symmetric about the midpoint of the reaction coordinate. Since figures 3.b and 6.c are mostly symmetric and bcc metals reflect a sinusoidal behavior [12], our case of study satisfies the conditions to use the 1/2 factor.

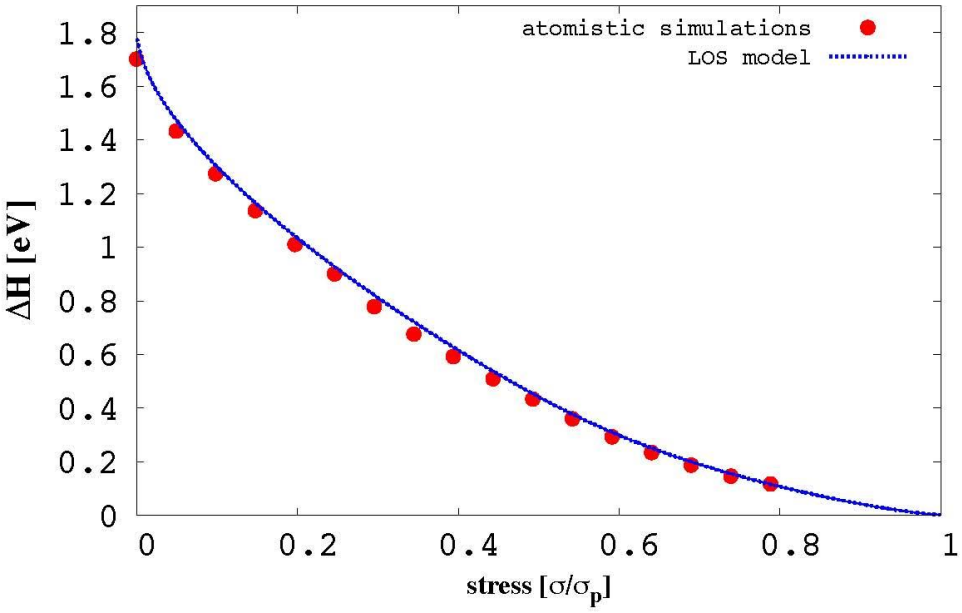

Figure 9: Kink-pair formation enthalpy comparing atomistic simulations using EAM potential and the LOS model fitted with the same potential.

The free energy can be defined as:

$$\Delta F_{kp} = \Delta H - T\Delta S$$

where ΔH is the enthalpy and ΔS the entropy. Assuming that the entropy can be taken as ΔS ~ 3k, the enthalpy is the missing variable to compute the nucleation rate of the kink-pair.

The atomistic data in Fig. 9 shows the dependence of the kink-pair enthalpy as a function of the applied stress. It results from obtaining, for each value of applied stress, the enthalpy of the point of intersection *A* in Fig. 7. As we expected, the value of the kink-pair enthalpy tends to zero when the applied stress is close to the Peierls stress.

To obtain the kink-pair enthalpy at 0 MPa the procedure developed by Ventelon et al. [14] was used, where 'the formation energy of a single kink is calculated as the difference between the energy of a kinked screw-dislocation and the energy normalized to the same number of atoms of a straight dislocation lying in a single Peierls valley'. The formation enthalpy (equivalent to the energy since there is no mechanical work at 0 MPa) of the kink-pair at 0 MPa is obtained as the sum of the formation enthalpies for the left and right kink. Fig.10 shows the convergence of the formation enthalpies with the number of atoms per plane perpendicular to the Burgers vector, obtaining a value of 1.701 eV for the EAM potential. Experimentally, Brunner [15] has obtained a value of 1.75 eV from the temperature dependence of flow stress measurements in W, in very good agreement with the calculated value.

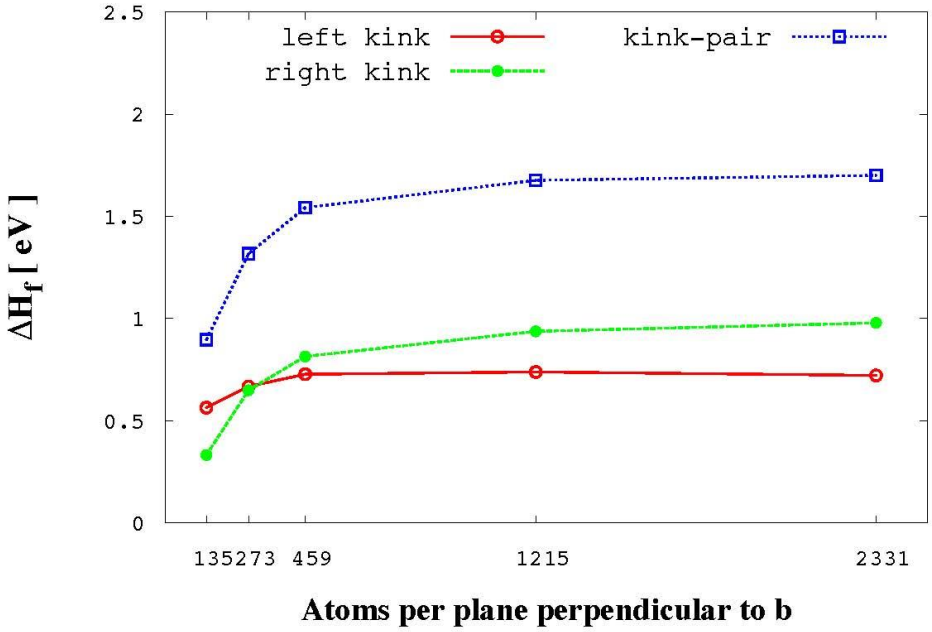

Figure 10: Kink formation enthalpies as a function of the number of atoms per Burgers vector.

3.3 Kink-Pair Width

As it was described in section 3.1, the study of the enthalpy barrier in kink-pairs requires that the initial path of the NEB simulation contains a single dislocation for the initial and final replica, while the intermediate replicas (2 . . . R-1) contain a kink pair of a specific width. The initial and final replicas maintain their dislocation shape after the NEB simulation. Some of the intermediate replicas achieve the minimum along the path in the form of a dislocation while some others keep the kink pair shape with a different width from the one that was imposed when defining the initial configurations of the intermediate replicas.

The envelope of minimum enthalpy represented in Fig. 7 gives an idea of when to expect the change of shape between dislocation and kink pair: intermediate replicas in regions 0-A and B-1 have a dislocation shape, whereas, intermediate replicas in region A-B have a kink pair shape. This can also be probed by visualizing the relaxed replicas via Ovito [16]. Figure 11 shows the results of this visualization, where the atoms defining the dislocation and the kink pair have been highlighted using the common neighbor analysis (CNA) technique [17, 18, 19].

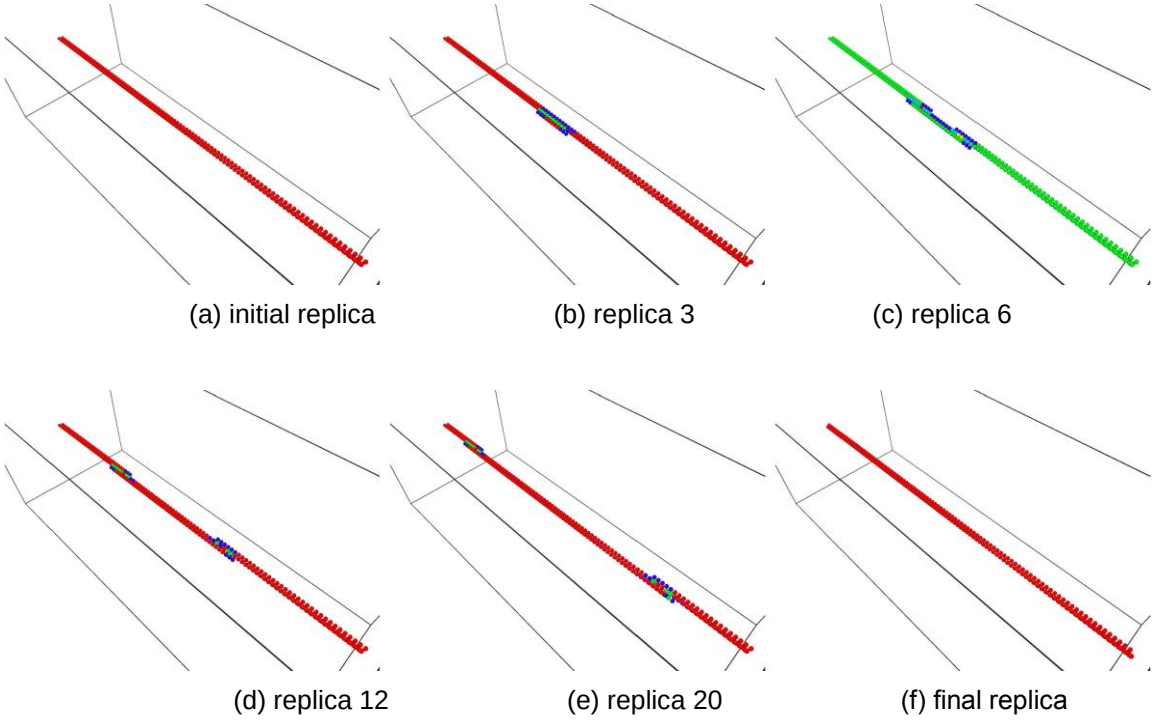

(a) initial replica (b) replica 3 (c) replica 6

(d) replica 12 (e) replica 20 (f) final replica

Figure 11: Atomistic visualization obtained via Ovito [16] of different replicas along the final pathway of the NEB simulation at 1200 MPa.

Atomistic visualizations of Fig. 11 using the CNA technique present kink pairs with a sharp shape and do not reproduce the details of their profile, required to determine the width. In order to obtain the details on the shape of the replicas, we suggest an analytical methodology that takes into account the coordinates of all the atoms in the simulation box and the displacement field associated with the dislocation.

The steps to obtain the shape of each replica with this analytical method suggested are:

- **i.** The simulation box is divided into slices along the dislocation line direction *x*. Each slice has a width of **b**/3 and contains the atoms of one single plane of the ABC stacking sequence of {111} planes in bcc metals.
- **ii.** For each slice, a grid of nodes that are candidates to host the centroid of the dislocation is created. The grid spacing would determine the efficiency of the method in terms of the precision of the results and the computational cost. The purpose is to identify between all the possible nodes in the grid, the node that is closer to the real position of the centroid of the dislocation.
- **iii.** Given a perfect bcc lattice oriented with *x*, *y* and *z* axes corresponding to the line, glide and normal directions respectively, inserting a screw dislocation in the box requires that every atom *i* is displaced according to the following field [3]:

$$u_x^i = \frac{b}{2\pi}\theta = \frac{b}{2\pi} tan^{-1}\left(\frac{R_z^i - c_z}{R_y^i - c_y}\right) \qquad (8)$$

$$u_y^i = y_z^i = 0$$

where R_x^i, R_y^i, R_z^i are the coordinates of an atom i in the perfect lattice and c_x, c_y, c_z are the coordinates of the centroid of the dislocation. Applying the previous displacement field to all the atoms in the box guaranties that the centroid of the dislocation is at $C(c_x, c_y, c_z)$.

If we want to obtain the centroid of a dislocation already inserted in a simulation box the previous process needs to be applied in reverse. Denoting r_x^i, r_y^i, r_z^i as the coordinates of an atom *i* in the distorted configuration with the screw dislocation, the centroid of the dislocation must satisfy the following condition for all the atoms *i* present in the slice:

$$r_x^i - R_x^i - \frac{b}{2\pi} tan^{-1}\left(\frac{R_z^i - c_z}{R_y^i - c_y}\right) = 0 \tag{9}$$

We then use as a measure error to locate the centroid. The displacement error on atom *i* when the centroid of the dislocation corresponds to node *n* is defined as:

$$\epsilon_n^i = r_x^i - R_x^i - \frac{b}{2\pi} tan^{-1}\left(\frac{R_z^i - R_z^n}{R_y^i - R_y^n}\right), \tag{10}$$

where R_x^n, R_y^n, R_z^n are the coordinates of the node *n*. Node *n* is considered the centroid of the dislocation for this slice if it minimizes, compared with all the other candidate nodes of the grid, the following sum:

$$\sum_{i=1}^{N_{at}} \epsilon_n^i \tag{11}$$

where N_{at} is the number of atoms in this slice.

iv. We repeat step (iii) for all slices and obtain the kink pair shape shown in Fig. 12.

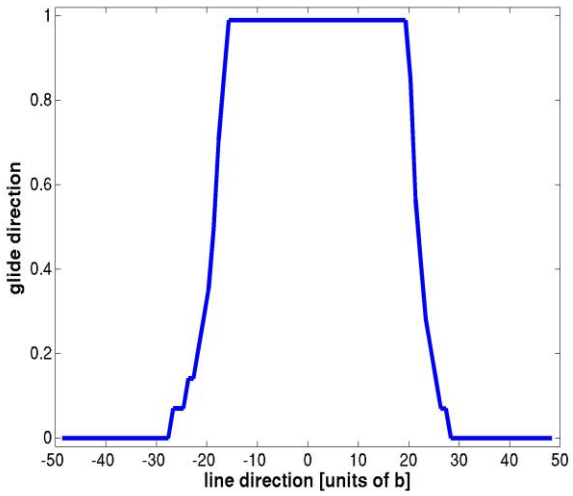

Figure 12: Shape of kink pair for replica number 14 of the reaction pathway at 1200 MPa.

It is important to consider that the positions of the centroid represented in Fig. 12 correspond only to the slices taken three by three, since the stacking sequence of {111} planes in bcc metals has three planes. The comparison between Fig. 11 and Fig. 12 reveals that the analytical method suggested provides the shape of the dislocation line with more detail than the atomistic visualizations.

Results from Fig. 13 shows that the initial and final replicas (1 and 31 respectively) maintain their dislocation shape, some of the intermediate replicas achieve the minimum along the path in the form of a dislocation (replicas number 4, 28) and some others keep the kink pair shape (replica numbers 5, 6, 7, 14, 21).

The enthalpy of the point of intersection *A* in Fig. 7 determines the kink pair enthalpy for each value of applied stress in Fig. 9. Therefore, ideally, the width of the kink pair should be computed at the same point *A*. However, replicas are spread along the reaction pathway in a linear way so it cannot be guaranteed that there is a replica that corresponds exactly with *A*. Consequently, the kink pair width is going to be computed from the first replica that exhibits a kink pair behavior with a fraction of the dislocation line totally positioned on the next valley.

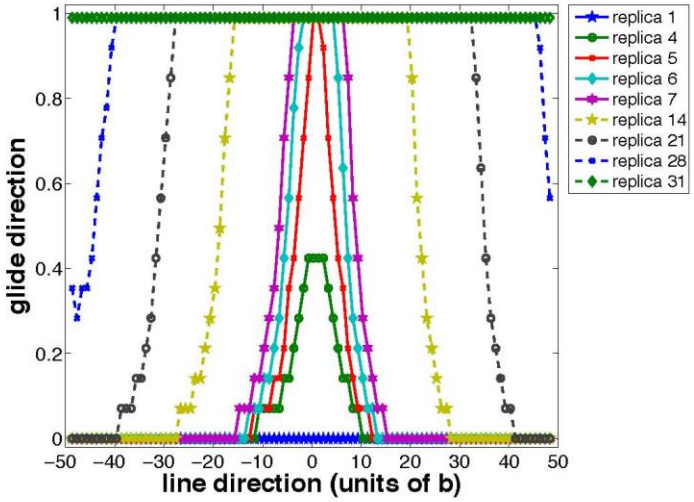

Figure 13: Shape of several replicas from the final pathway of the NEB simulation when applying 1200 MPa.

Once the replica with the first kink pair behavior is selected, the kink pair width is measured between the inflection points of the two legs of the kink pair. When repeating this process for all the values of applied stress, Fig. 14 is obtained.

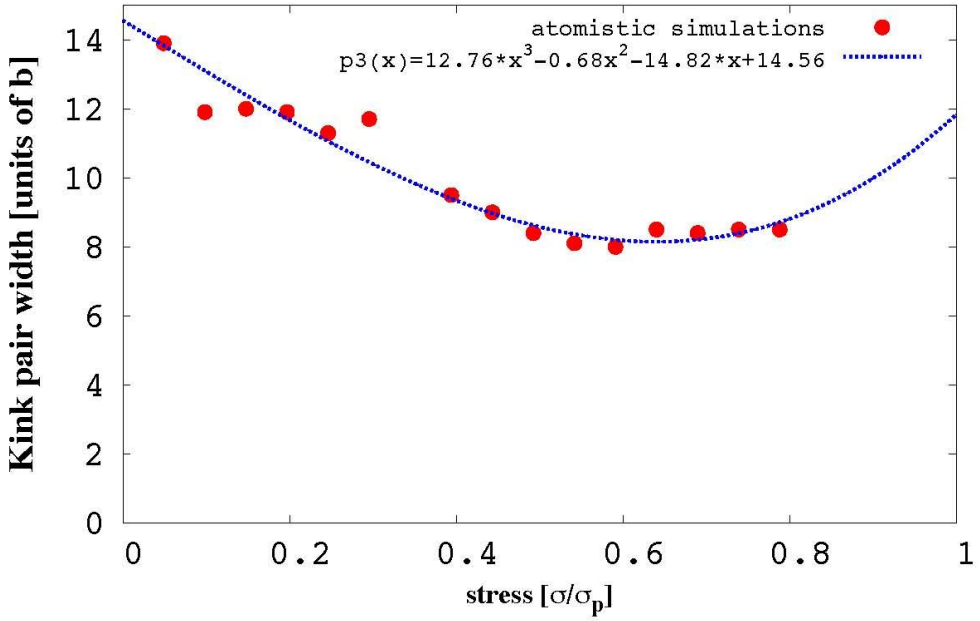

Figure 14: Kink pair width as a function of the applied stress.

Acknowledgments

This work was performed in part under the auspices of the U.S. Department of Energy by Lawrence Livermore National Laboratory under Contract DE-AC52-07NA27344. Document number LLNL-TR-666244.

References

[1] *Methods for Finding Saddle Points and Minimum Energy Paths*. G. Henkelman, G. Jöhannesson, and H. Jönsson. Kluwer Academic Publishers, 2000.

[2] Ellad B. Tadmor and Ronald E. Miller. *Modeling Materials, Atomistic and Multiscale Techniques*. Cambridge University Press, 2011.

[3] D. Hull and D. J. Bacon. *Introduction to Dislocations*. Butterworth-Heinemann, Oxford, 2001.

[4] S. Plimpton. *Fast Parallel Algorithms for Short-Range Molecular-Dynamics*. http://lammps.sandia.gov. Journal Of Computational Physics, 117(1):1-19, 1995.

[5] G. Henkelman, B.P. Uberuaga, and H. Jonsson. A climbing image nudged elastic band method for finding saddle points and minimum energy paths. *Journal of Chemical Physics*, 113(22):9901-9904, 2000.

[6] G. Henkelman and H. Jonsson. Improved tangent estimate in the nudged elastic band method for finding minimum energy paths and saddle points. *Journal of Chemical Physics*, 113(22):9978-9985, 2000.

[7] Aiichiro Nakano. A space-time-ensemble parallel nudged elastic band algorithm for molecular kinetics simulation. *Computer Physics Communications*, 178(4):280-289, 2008.

[8] Mihai-Cosmin Marinica et al. Interatomic potentials for modelling radiation defects and dislocations in tungsten. *Journal of Physics: Condensed Matter*, 25, 395502, 2013.

[9] Hyoungki Park, Michael R. Fellinger, Thomas J. Lenosky, William W. Tipton, Dallas R. Trinkle, Sven P. Rudin, Christopher Woodward, John W. Wilkins, and Richard G. Hennig. Ab initio based empirical potential used to study the mechanical properties of molybdenum. *Phys. Rev. B*, 85:214121, 2012.

[10] L. Proville, L. Ventelon, and D. Rodney. Prediction of the kink-pair formation enthalpy on screw dislocations in α-iron by a line tension model parametrized on empirical potentials and first-principles calculations. *Physical Review B*, 87(14):144106, 2013.

[11] D. Cereceda, A. Stukowski, M. R. Gilbert, S. Queyreau, Lisa Ventelon, M-C Marinica, J. M. Perlado, and J. Marian. Assessment of interatomic potentials for atomistic analysis of static and dynamic properties of screw dislocations in W. *Journal of Physics-Condensed Matter*, 25(8):085702, 2013.

[12] Christopher R. Weinberger, Garritt J. Tucker, and Stephen M. Foiles. Peierls potential of screw dislocations in bcc transition metals: Predictions from density functional theory. *Physical Review B*, 87(5):054114, 2013.

[13] David Rodney and Laurent Proville. Stress-dependent Peierls potential: Influence on kink-pair activation. *Physical Review B*, 79(9):194108, 2009.

[14] L. Ventelon, F. Willaime, and P. Leyronnas. Atomistic simulation of single kinks of screw dislocations in α-fe. *Journal of Nuclear Materials*, 386-388(C):26-29, 2009.

[15] D Brunner. Comparison of ow-stress measurements on high-purity tungsten single crystals with the kink-pair theory. *Materials Transactions JIM*, 41(1):152-160, 2000.

[16] Alexander Stukowski. Visualization and analysis of atomistic simulation data with OVITO-the Open Visualization Tool. *Modelling and Simulation in Materials Science And Engineering*, 18(1), JAN 2010.

[17] J. Dana. Honeycutt and Hans C. Andersen. Molecular dynamics study of melting and freezing of small Lennard-Jones clusters. *The Journal of Physical Chemistry*, 91(19):4950-4963, 1987.

[18] Daniel Faken and Hannes Jnsson. Systematic analysis of local atomic structure combined with 3d computer graphics. *Computational Materials Science*, 2(2):279-286, 1994.

[19] Helio Tsuzuki, Paulo S. Branicio, and Jos P. Rino. Structural characterization of deformed crystals by analysis of common atomic neighborhood. *Computer Physics Communications*, 177(6):518-523, 2007.